One-step synthesis of gold nanoparticles for catalysis and SERS applications using selectively dicarboxylated cellulose and hyaluronate

One-step synthesis of gold nanoparticles for catalysis and SERS applications using selectively dicarboxylated cellulose and hyaluronate

Alžběta Vávrová, Tereza Čapková, Ivo Kuřitka, Jan Vícha [*], Lukáš Münster[*]

Centre of Polymer Systems, Tomas Bata University in Zlín, tř. Tomáše Bati 5678, 760 01 Zlín, Czech Republic

Email: munster@utb.cz, jvicha@utb.cz

Abstract:

Properties and applications of gold nanoparticles (AuNPs) depend on their characteristics intrinsically connected to the reducing and capping agents used in their synthesis. Although polysaccharides are commonly used for Au salt reduction, the control over the result is often limited. Here, the selectively dicarboxylated cellulose (DCC) and hyaluronate (DCH) with adjustable composition and molecular weight are used for the first time as reducing and capping agents for AuNPs preparation in an environmental friendly one-step synthesis. Mechanism of reduction and structure-function relationships between the composition of oxidized polysaccharides and properties of formed AuNPs are elucidated and the variances in the macromolecular architecture of dicarboxypolysaccharides are applied to guide the growth of AuNPs. While the homogenous structure and high density of carboxyl groups of fully-oxidized DCC induced isotropic growth of small and uniform AuNPs with good catalytic performance (d=~20nm, TOF=7.3min^{-1}, k=1.47min^{-1}), the lower stabilizing potential and slower reduction rates of the DCH induced the anisotropic growth of larger polyhedral ~50nm nanoparticles, which excelled increased the Surface-Enhanced Raman Scattering efficacy (9× stronger Raman signals on average compared to AuDCC). The use of dicarboxypolysaccharides with adjustable composition and properties thus introduced a new degree of freedom for the preparation of AuNPs with desired properties.

Keywords: dicarboxypolysaccharides; dicarboxylated cellulose; dicarboxylated hyaluronate; gold nanoparticles; surface-enhanced Raman scattering; catalysis;

1. Introduction

Gold nanoparticles (AuNPs) have been attracting considerable attention due to their potential applications as sensors [1,2], for visualization and labeling [3], as biological/pharmaceutical devices and drug delivery vehicles [4], or as catalysts [5,6] and diverse biomedical applications [7–9]. Such a broad span of potential applications is allowed by the intrinsic connection between characteristics of AuNPs and their size, shape, and surface modifications [10]. For instance, the Surface-Enhanced Raman Scattering (SERS) effect, which is exploited in highly sensitive techniques for chemical and bioanalytical sensing and imaging [11], can be improved by several orders of magnitude by adsorption of analyzed molecules on the surface of gold nanoparticles. The actual enhancement factor depends on the size of nanoparticles as well as on their shape and surface features [11,12]. When spherical AuNPs are considered, maximum enhancement is obtained for AuNPs of the size of about 50 nm [13]. However, nanoparticles with uneven shapes and irregular surfaces usually provide far better results than similarly sized spherical ones, as the presence of edges or points on nanoparticle surfaces creates electromagnetic "hot-spots", which amplifies the Raman signal of the analyte molecule [14].

The size of AuNPs has a major impact also on their catalytic performance [5,6]. In contrast to SERS, the catalytic activity of AuNPs diminishes considerably with increasing particle size; the best results are obtained using sub-10 nm AuNPs [15]. For instance, AuNPs can efficiently catalyze the oxidation of carbon monoxide at low temperatures, convert alcohols to aldehydes, hydrogenate alkenes and nitro groups or oxidize volatile organic compounds [15–17]. They are even investigated as potential "green catalysts" because supported AuNPs are capable of efficient aerobic oxidation of benzylic, allylic and aliphatic primary and secondary alcohols with water as the only byproduct [15,17].

Rather contradictory requirements for AuNPs properties led to the development of many synthetic methods designed to prepare AuNPs of different shapes and sizes (spheres, rods, stars, flowers, urchins, *etc.*) [18–20]. The growing interest in the environmentally benign synthesis of AuNPs eventually led to the development of synthetic routes that involve polysaccharides and their derivatives. Polysaccharides are biocompatible and renewable materials that conveniently allow for one-step green synthesis of AuNPs because they simultaneously act as both reducing and capping agents. The exact relationship between the polysaccharide structure and properties of resulting AuNP, although not yet fully understood, is known to be influenced by the molecular weight of the polysaccharide and the type and amount of functional groups in their structure [15,21]. In essence, the molecular weight of the polysaccharide reflects the number of reducing-end groups, which initiate the reduction of Au^{III} salts. The amount of –OH, $–NH_2$, and –COOH groups of the polysaccharide that can attach to the surface of growing nanoparticles by covalent, electrostatic, weak, or dispersion interactions then influences their stabilization against aggregation [22]. Hence, by controlling the molecular weight and composition of polysaccharides it should be possible to better guide the growth of AuNPs towards desired applications.

Here, regioselectively oxidized dicarboxypolysaccharides (DCPs) are employed for the first time as reducing and capping agents in AuNPs synthesis, and the differences in their macromolecular architecture are applied for guiding the growth of AuNPs towards enhancement of catalytic and SERS efficacies. DCPs are prepared using a two-stage oxidation scheme, in which a pair of hydroxyl groups on neighboring carbon atoms (vicinal diol) is initially oxidized by sodium periodate into a pair of –CHO groups, which are

further oxidized by sodium chlorite to carboxylates as depicted in Figure 1 [23,24]. The use of DCPs has several key advantages over the current methods employing only the periodate-oxidized dialdehyde polysaccharides (DAPs), such as dialdehyde nanocelluloses [25–27], which feature a highly complex composition composed of a mixture of various intra- and intermolecular hemiacetals [28]. Further oxidation used in DCP preparation i) improves the material composition by disrupting the hemiacetals in DAPs [29], ii) introduces a pair of –COOH groups in each oxidized unit capable of efficient stabilization of Au clusters and nanoparticles [30], iii) allows for easy control over the molecular weight of DCPs. The last is achieved by the recently developed sulfonation-induced chain scission method based on the addition of sulfamic acid into the reaction mixture, which leads to controlled hydrolysis of DCP chains [24,29]. Hence, by the careful selection of source materials, modification of primary (periodate) oxidation, which dictates the degree of oxidation (*DO*), and by the adjustment of molecular weight during secondary oxidation, one could obtain DCPs featuring the well-defined structure of oxidized units, distinctly different architecture of macromolecular chains, variable *DO* and adjustable molecular weight, all of which can influence the growth of AuNPs. The whole process is schematically summarized in Figure 1.

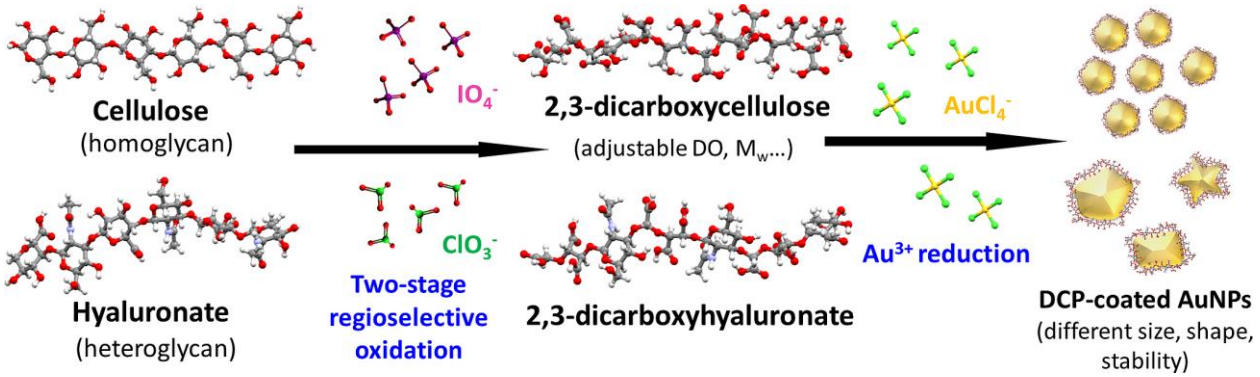

Figure 1 The overall scheme of proposed AuNPs synthesis using dicarboxypolysaccharides (DCPs). Briefly, different polysaccharides are regioselectively oxidized into respective DCPs, which are used for the reduction of Au^{III} salt and preparation of AuNPs of different characteristics, depending on the structure and properties of DCPs and source polysaccharides.

In this work, the advantages of the proposed method are demonstrated using two distinctly different polysaccharides, the cellulose, a homoglycan composed of D-anhydroglucose units (AGU) connected by β-1→4 glycosidic linkages, and the sodium hyaluronate (HA), a heteroglycan composed of D-glucuronic acid and N-acetyl-D-glucosamine bound by alternating β-(1→4) and β-(1→3) glycosidic linkages. These source materials were oxidized to 2,3-dicarboxylated cellulose (DCC) and 2,3-dicarboxylated hyaluronate (DCH), respectively, and employed for the preparation of AuNPs, which SERS and catalytic efficacies were evaluated. Besides, the mechanism of gold salt reduction by DCPs was elucidated and the relationship between DCP structure and properties of AuNPs was investigated to guide future efforts.

2. Experimental Section

2.1 Materials

Oxidized polysaccharides (2,3-dicarboxylated cellulose DCC and 2,3-dicarboxylated hyaluronate DCH) were prepared from Sigmacell Type 20 cellulose (weight-average molecular weight M_w = 76 kDa, polydispersity

index *PDI* = 4.7, degree of polymerization *DP* = 468) and sodium hyaluronate (HA, M_w = 396 kDa, *PDI* = 5.9, *DP* = 987) (Contipro, Czech Republic) by sequential oxidation. This process included sodium periodate ($NaIO_4$) (Penta, Czech Republic), ethylene glycol (Sigma Aldrich, Co.), sodium hydroxide (NaOH) (Lachner, Czech Republic), hydrochloric acid (HCl) (Penta, Czech Republic), sodium chlorite ($NaClO_2$) (Penta, Czech Republic), acetic acid (CH_3COOH) (Sigma Aldrich Co.) and pH 4.5 acetic buffer composed of 0.045 mol/L sodium acetate trihydrate ($CH_3COONa{\cdot}3H_2O$) (Penta, Czech Republic) and 0.055 mol/L CH_3COOH. Sodium nitrate ($NaNO_3$) (Lachner, Czech Republic) and disodium hydrogen phosphate dodecahydrate ($Na_2HPO_4{\cdot}12H_2O$) (VWR, Czech Republic) were used in the characterization of prepared polysaccharide derivatives. Gold(III) chloride trihydrate ($HAuCl_4{\cdot}3H_2O$) (Sigma Aldrich Co.) was used as an AuNPs precursor. For the testing of catalytic and SERS activity, sodium borohydride ($NaBH_4$), 4-nitrophenol (4-NP), and N-acetylcysteine (NAC) (Sigma Aldrich, Co.) were used, respectively. All used chemicals were of analytical purity (p.a.) and used as received without further purification. Demineralized water was used throughout the experiment.

2.2 Preparation of oxidized polysaccharides

DCC and DCH were prepared by sequential oxidation following previous work [24]. Briefly, initial periodate oxidation of cellulose was performed at 30 °C for 16 h (partially oxidized) and 72 h (fully oxidized) using a 1:1.2 molar ratio between cellulose and $NaIO_4$. The degree of oxidation after periodate oxidation, *i.e.* the percentage of oxidized units, was estimated by observing the decrease of the intensity of periodate ion absorption peak at 220 nm in UV/VIS spectra after given times (Figure 2). The UV-Vis spectral analysis was further correlated with findings from an NMR study performed on DCPs. Oxidation of HA was performed for 24 h using a 1:3.1 molar ratio of HA : $NaIO_4$. All reactions were conducted in the absence of light. Excess of ethylene glycol was added to terminate the reaction by decomposing the residual periodate. Dialdehydecellulose was purified by repeated centrifugation and mechanical homogenization, while the soluble dialdehyde hyaluronate was purified by dialysis against demineralized water using 14 kDa molecular-weight cut off (*MWCO*) membrane (Sigma Aldrich, Co.). Samples were filtered, flash-frozen (-80 °C), and lyophilized. Secondary oxidation of both dialdehyde derivatives was carried out using sodium chlorite at 30 °C in an acidic environment in the absence of light and under vigorous stirring. Secondary oxidation of dialdehyde cellulose was performed for 7 h using a 1:4:2 molar ratio of −CHO : $NaClO_2$: CH_3COOH with the concentration of $NaClO_2$ and CH_3COOH set to 1 and 0.5 mol/L, respectively. Secondary oxidation of dialdehyde hyaluronate was performed for 24 h using the similar setup with the following adjustments: i) the acetic acid was replaced by acetate buffer composed of 0.045 mol/L $NaCH_3COOH$ and 0.055 mol/L CH_3COOH (pH 4.5), ii) concentration of oxidizing agent was lowered down to 0.2 mol/L and iii) duration was prolonged to 24 h. These modifications were employed to reduce the degradation of dialdehyde hyaluronate while retaining high conversion from –CHO to –COOH during secondary oxidation.

Both reactions were terminated by the addition of NaOH (pH 8) and the product was dialyzed against demineralized water for 48 h. After dialysis, the pH of the resulting dicarboxypolysaccharide solutions was adjusted to 7.4 with 0.1 mol/L NaOH, samples were filtered and lyophilized. Resulting 2,3-dicarboxylated cellulose (DCC), partially oxidized 2,3-dicarboxylated cellulose (DCC-70) and 2,3-dicarboxylated hyaluronate (DCH) were obtained as sodium salts.

2.3 Synthesis of AuNPs using dicarboxypolysaccharides

Initially, a screening of reaction conditions was performed. The general procedure for the synthesis of AuNPs starts with dissolving a given amount of source DCP in water, followed by the addition of a gold solution containing 5 mg of $HAuCl_4 \cdot 3H_2O$ and the addition of a given amount of NaOH. The reaction mixtures in light-sealed vials were vortexed, placed into an oil bath, heated up to 90 °C, and shaken for several hours. The total volume of reaction mixtures was 10 mL. Samples were then collected, filtered, and analyzed. The effect of synthesis duration on properties of prepared AuNPs (A-series of samples) was tested on samples with weight concentration of DCP arbitrary set to 0.8 wt% and molar concentration of NaOH set to 5 mmol/L. The aliquots were collected each hour for 5 h. Next, the effect of polysaccharide weight concentration (B-series of samples, concentration range 0.2–1.2 wt%) was investigated. The duration of syntheses was set to 3 h for both DCC-70 and DCC but 5 h for DCH, based on A-series results (see Section *3.3*). The C-series samples were used to investigate the effect of the concentration of NaOH in reaction media (0 mmol/L to 10 mmol/L). All results are summarized in Supporting Information (SI). Codification of all prepared AuNPs samples is given in Table S1. It includes the series code (A, B or C), type of polysaccharide (DCC-70, DCC or DCH), duration of synthesis (t = 1–5 h), weight concentration of DCP (w = 0.2–1.2 wt%) and molar concentration of NaOH (c = 0–10 mmol/L). For example, in A_AuDCC-70_t1_w08_c5, the A stands for A-series, AuDCC-70 indicate that DCC-70 has been used for AuNP synthesis, t1 stands for reaction time 1 h, w08 for 0.8 wt% concentration of DCP, and c5 for c_{NaOH} = 5 mmol/L concentration of NaOH.

Based on screening study, production samples were prepared using t = 3 h, w_{DCC} = 0.6 wt%, c_{NaOH} = 5 mmol/L for AuDCC sample; t = 3 h, $w_{DCC\text{-}70}$ = 0.4 wt%, c_{NaOH} = 5 mmol/L for AuDCC-70 sample and t = 5 h, w_{DCH} = 0.4 wt%, c_{NaOH} = 5 mmol/L for AuDCH sample, while the amount of $HAuCl_4 \cdot 3H_2O$ and total reaction volume remained the same as before. These parameters were selected based on the size, shape, and Zeta potential of AuNPs. Samples were purified by filtration and repeated centrifugation at 4 000 rpm and characterized using methods described below.

2.4 Characterization of dicarboxypolysaccharides

Ultraviolet–visible spectroscopy (UV-Vis). To monitor the change of the *DO* during periodate oxidation, spectral analysis was carried out using a double-beam UV-Vis spectrometer Lambda 1050 (PerkinElmer, USA) in the span of 180−500 nm. The decrease of the intensity of periodate ion absorption peak at 220 nm was recorded during 72 h oxidation reaction. This was done by measuring intensity aliquots collected at given times.

Infrared spectroscopy (FT-IR). Qualitative spectral analysis was conducted on the prepared DCPs and source polysaccharides employing FT-IR spectrometer Nicolet 6700 (Thermofisher Scientific, USA) equipped with diamond crystal operated in ATR mode in the span of wavenumber ranging from 4000 to 400 cm^{-1}. All FT-IR spectra can be found in SI (Figure S1).

X-ray diffraction analysis (XRD). The crystallinity of the source polysaccharides and prepared DCPs lyophilizes was examined by a Rigaku MiniFlex600 X-ray diffractometer in the diffraction 2θ angle range 5–95°, CoKα (λ = 1.789 Å) radiation source was used with Kβ line filter. All XRD diffractograms can be found in SI (Figure S2). Williamson-Hall method was used for the calculation of crystallite sizes.

Viscosity measurements. Dynamic viscosity (η^*) of the prepared DCPs solutions (0.2 and 1.2 mg/mL) was measured using a rotational rheometer Anton Paar MCR 502 (Anton Paar, Austria) equipped with a double-gap measuring system (DG26.7). All experiments were done at 25 °C in oscillation mode employing angular frequency sweep from 0.1 to 10 s^{-1} and applying constant strain of 1 %. All viscosity measurements can be found in SI (Figure S3).

Nuclear magnetic resonance (NMR). ^{1}H spectra of the prepared DCPs and the changes in DCPs structure after blank AuNPs synthesis experiment (*i.e.* the exact synthesis procedure without the presence AuNPs precursor but with an equivalent amount of HCl instead) were recorded using Bruker Avance III HD 700 MHz NMR spectrometer (Bruker, USA) equipped with a triple-resonance cryoprobe at 298 K in D_2O. *DO* of oxidized cellulose, *i.e.* the percentage of AGU converted to 2,3-dicarboxylated cellulose units, was determined from ^{1}H NMR spectra by comparing the average of H4 and H5 signal intensities (3.98–4.03 ppm, signals of oxidized units) with the sum of the signals at 4.43 ppm and 4.95 ppm, which were identified as H1' of non-oxidized cellulose units neighboring charged oxidized moieties (4.95 ppm) [29,31] and as H1' of non-oxidized cellulose units with non-oxidized neighbors [32]. The *DO* of prepared DCH samples was determined by the comparison of signal intensities of H4 and H5 from oxidized glucuronic acid units (4.07 and 4.19 ppm) and well-separated signal H5' (3.48 ppm) of intact N-acetyl-D-glucosamine unit, which is resistant to periodate oxidation. Hence, if both signal intensities would be equal, the glucuronic acid would be fully oxidized.

Gel permeation chromatography (GPC). The molecular weight distribution and the changes in DCPs molecular weight distributions after the blank AuNPs synthesis of the prepared DCPs were analyzed by gel permeation chromatography (GPC) using a Waters HPLC Breeze chromatographic system (Waters, USA). Refractive index detector Waters 2414 (drift tube T = 60 °C), Tosoh TSK gel $GMPW_{XL}$ column (300 mm × 7.8 mm × 13 µm, column T = 30 °C) was employed towards this purpose. The mobile phase consisted of a mixture of 0.1 mol/L $NaNO_3$ and 0.05 mol/L $Na_2HPO_4{\cdot}12H_2O$. Pullulan polysaccharide calibration kit SAC-10 (M_w 342–805 000 g/mol, Agilent Technologies, USA) was used.

2.5 Characterization of AuNPs

Ultraviolet−visible spectroscopy (UV-Vis). The local surface plasmon resonance (LSPR) of AuNPs samples was estimated by a double-beam UV-Vis spectrometer Lambda 1050 (PerkinElmer, USA) in the span of 350−800 nm. The LSPR absorption band of AuNPs occurs from 500 nm to 600 nm according to the size of nanoparticles. The full width at half maximum (FWHM), which reflects particle size distribution, was also investigated.

Transmission electron microscopy (TEM). TEM was conducted using a JEM-2100 transmission microscope (JEOL, Japan) operated at an acceleration voltage of 160 keV. The samples were drop-cast from diluted aqueous suspension onto 300 mesh copper grid coated with Formvar membrane and gently dried.

Thermogravimetric analysis (TGA). To estimate the mass of DCPs in stabilizing layer on the surface of AuNPs, TGA analyses were carried out on purified AuNPs samples (*i.e.* production samples) and corresponding DCPs as reference blank samples. The ratios between the stabilizing layer of DCPs and AuNPs core were estimated by subtraction of respective TGA curves. Thermal characteristics were measured using a LabSys Evo DTA/DSC thermogravimeter (Setaram Instrumentation, France) equipped

with a TGA sensor employing corundum crucibles a temperature range of 30–800 °C and heating rate 5 °C/min; the weight of each sample was about 5 mg. As carrier gas, the air was used during measurements (flow 60 mL/min).

X-ray diffraction analysis (XRD) and X-ray fluorescence (XRF). The crystallinity of AuNPs production samples was analyzed by XRD as described in section *2.4*. The concentration of Au in selected and purified AuNPs samples (*i.e.* production samples) was determined by an energy-dispersive X-ray fluorescence spectrometer by ARL Quant'X EDXRF Analyzer (Thermo Scientific, USA). For the determination of Au amount in the samples, the calibration standards were prepared by dissolving a defined amount of $HAuCl_4 \cdot 3H_2O$ solution in water.

Dynamic light scattering (DLS). Zeta potential (*ζ*) of all AuNPs samples was determined by dynamic light scattering (DLS) on a Zetasizer Nano ZS90 instrument (Malvern Instruments, UK) at 25 °C using DTS1070 cells and Smoluchowski model. Moreover, ζ potentials and hydrodynamic radii in pH range 2–12 were investigated for selected AuNPs samples (*i.e.* production samples). The pH during measurements was adjusted employing 0.1 and 0.01 mol/L NaOH and 0.1 and 0.01 mol/L HCl solutions. The concentration of AuNPs in the samples was 0.05 mg/mL.

Surface-enhanced Raman scattering (SERS). DXR Raman microscope (Thermo Scientific, USA) was used to determine the effect of AuNPs production samples on the Raman signal of NAC, which was used as a model molecule. Neat AuNPs and NAC solutions were used as blank samples. Raman spectra were recorded at a NIR excitation wavelength (780 nm) with laser power 3 mW and in the span 3400–500 cm^{-1}. Three mixtures containing 0.1 mg/mL AuNPs (AuDCC, AuDCC-70, and AuDCH) and 2 mg/mL of NAC were shaken at 37 °C for 24 h in the dark. Spectra were collected on an aluminum substrate containing 50 µL of each dried sample mixture.

The catalytic activity of prepared AuNPs was investigated by catalytic reduction of 4-nitrophenol (4-NP) to 4-aminophenol (4-AP) by sodium borohydride [33]. The reaction was carried out as follows: a solution containing 20 µg of AuNPs was added to the aqueous solution containing 0.5 mmol of 4-NP (c = 0.17 mmol/L, $n_{AuNPs} : 5n_{4\text{-}NP}$) and 12.5 mmol of sodium borohydride (c = 66 mmol/L). The reduction of 4-NP was investigated at 25 °C by observing the decrease of 4-NP UV-Vis absorbance at 400 nm using double-beam UV-Vis spectrometer Lambda 1050 (PerkinElmer, USA) until constant absorbance values. Reduction reaction follows pseudo-first-order kinetics and rate constants (k) were determined as a slope of $ln(C_t/C_0)$ plotted vs. time. The blank experiment was performed under similar conditions; the AuNPs were replaced by an equivalent amount of given DCP to rule out potential side reactions with the substrate. Note that, although the AuNPs also absorb at 400 nm, their absorbance at a given concentration was not observable and thus neglected. The turnover frequencies (TOFs) of AuNPs, which correspond to moles of reactant converted by given molar amount of catalyst per minute (min^{-1}) at 25 °C, were calculated according to Kozuch and Martin [34] and are expressed concerning the initial concentration of 4-NP.

3. Results and Discussion

3.1 Preparation and characterization of dicarboxypolysaccharides

Primary oxidation of cellulose was investigated by observing the periodate ion consumption, which relates to the degree of oxidation of a given polysaccharide, Figure 2. Briefly, periodate ion exhibits absorption in the UV-Vis region around 220 nm. As the oxidation proceeds, the intensity of this band decreases with the consumption of the oxidation agent. As 1 mole of $NaIO_4$ is used to convert 1 mole of AGU units (overoxidation of end groups is neglected), the oxidation degree, *i.e.* the percentage of AGU units oxidized by periodate, can be directly determined. Moreover, the stability of the periodate was evaluated in the blank experiment (without polysaccharides). The decomposition of periodate over 96 h was below 5 %, which is comparable to experimental error (dashed line in Figure 2). Besides highly oxidized DCC (duration of primary oxidation 72 h, green squares in Figure 2), partially oxidized cellulose was also prepared. The target *DO* was set to 70 %, which should still ensure good solubility of the product while simultaneously introducing significant heterogeneity into its structure. The duration of primary oxidation was thus set to 16 h based on periodate ion consumption (red squares in Figure 2). Partially oxidized cellulose, referred to as DCC-70 in the following text, was prepared to i) demonstrate the possibility of the control over the *DO* of the polysaccharide, ii) investigate the influence of irregular chain structure composed of randomly distributed oxidized and non-oxidized units on properties of AuNPs.

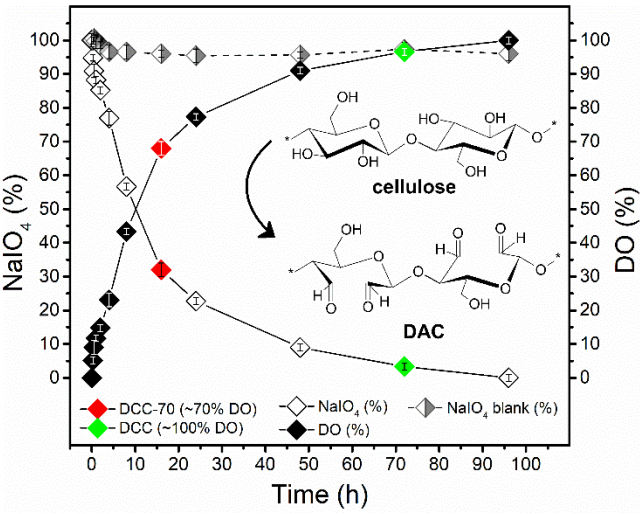

Figure 2 The consumption of $NaIO_4$ as a function of time during the periodate oxidation of cellulose (left Y-axis). The second plot depicts a related degree of oxidation achieved by primary periodate oxidation (right Y-axis). The dashed line illustrates the stability of $NaIO_4$ in blank experiment (without polysaccharide).

All prepared DCPs were characterized by FT-IR and XRD and their solutions were investigated by viscosimetric, ^1H NMR, and GPC analysis. The oxidation of polysaccharides is manifested in FT-IR spectra of prepared DCPs, as well as source cellulose and hyaluronate (Figure S1), by the appearance of a C=O absorption band about 1600 cm^{-1} for DCC derivatives and the increase of intensity of this vibration in DCH spectra, respectively. The latter is caused by the fact that selective oxidation essentially triples the number of carboxyl groups in DCH. The XRD diffractograms of source polysaccharides and DCPs (Figures S2A and B) revealed complete disruption of cellulose crystalline structure after the 72 h of oxidation, manifested by disappearing or significant broadening of formally sharp diffraction peaks at 2θ around 18°, 26°, and 40°. This observation is well in line with previous literature findings [28]. There is only a small difference

between DCC and DCC-70 diffractograms – DCC-70 exhibits a slightly sharper diffraction pattern at 2θ around 26°, which correlates with a larger number of residual unoxidized AGU units. No change in crystallinity between already amorphous HA and DCH was observed.

The DCPs solutions were further characterized in the terms of change in dynamic viscosity η^* (Figure S3), but no significant differences were observed between the low (0.2 wt%) and the high (1.2 wt%) concentration; the values were around 60±10 mPa.s at angular frequency 0.1 s^{-1}. The only exception is the DCC-70 solution, which is slightly less viscous (38 mPa.s at ω = 0.1 s^{-1}) at 0.2 wt% concentration. The oxidation of –OH groups to –COOH thus results in DCP solutions of rather low viscosity. This is likely a result of DCP chains repulsion due to the high negative charge in combination with the higher flexibility of oxidized chains given by the disruption of the C2-C3 bond.

The ^{1}H NMR spectra and structures of DCH and fully/partially oxidized DCC are given in Figure 3. For ^{13}C and ^{1}H-^{13}C NMR spectra of DCC and DCH, as well as full signal assignment, see our previous works. [24,29,31] Obtained ^{1}H NMR spectra well illustrate the different nature of each DCP. The presence of four distinct signals of H1, H4, H5, and H6 (there are no protons on C2 and C3) in the spectra of DCC indicates a well-defined structure composed of 2,3-oxidized AGU units connected by β-(1→4) glycosidic linkages. Note that the signal of H1 overlaps with the signal of the solvent and is thus not visible in the spectra. Only traces of non-oxidized AGU signals are visible, see for instance signals at 4.95 ppm or the region between 3.2–3.6 ppm; DCC is thus considered to be fully oxidized.

Besides mentioned four main signals of H1, H4, H5, and H6 from oxidized units, whose chemical shifts slightly differ from those found in DCC likely due to the presence of nearby non-oxidized units, the ^{1}H NMR spectrum of partially oxidized cellulose DCC-70 also contains the signals of non-oxidized AGU (*e.g.* 4.95, 4.43, 4.15, 4.14, 3.59 ppm, 3.33 and 3.25 ppm). Note, that the signals of chemically equivalent protons in the AGUs may be significantly shifted depending on their chemical surroundings, *i.e.* whether they are neighboring with oxidized or non-oxidized units. For instance, signals at 4.95 and 4.43 ppm both belong to H1' neighboring with oxidized and un-oxidized units, respectively [29,31,32]. This was taken into consideration in the calculation of *DO*, which was established based on the sum of H1' signals to be 70 %, thus confirming findings from UV/VIS measurements. In other words, approximately every third cellulose unit remains non-oxidized.

The spectrum of DCH contains three signals of oxidized D-glucuronic acid unit (4.07, 4.19, 4.47 ppm) and six signals of intact N-acetyl-D-glucosamine unit (signal of $-CH_3$ group at 1.92 ppm is not shown for the sake of better resolution). The ^{1}H NMR spectrum of HA was added for comparison. The oxidation of D-glucuronic acid groups is, for instance, evident from the disappearance of the H2 signal at 3.27 ppm and the shift of the H1 signal from 4.38 ppm to 4.47 ppm, respectively. Although some of N-acetyl-D-glucosamine unit signals are shifted after oxidation of glucuronic acid groups, particularly the H1', their overall pattern is consistent with the resistance of N-acetyl-D-glucosamine unit to periodate oxidation in agreement with previous findings [24]. The DCH thus features the most complex structure from all investigated systems, comprising of highly charged oxidized D-glucuronic acid groups alternating with less polar non-oxidized N-acetyl-D-glucosamine units. The *DO* of DCH was determined to be 92 % with the remaining 8 % likely composed of stable hemiacetals formed after primary oxidation, which remained intact even during oxidation by chlorite [24].

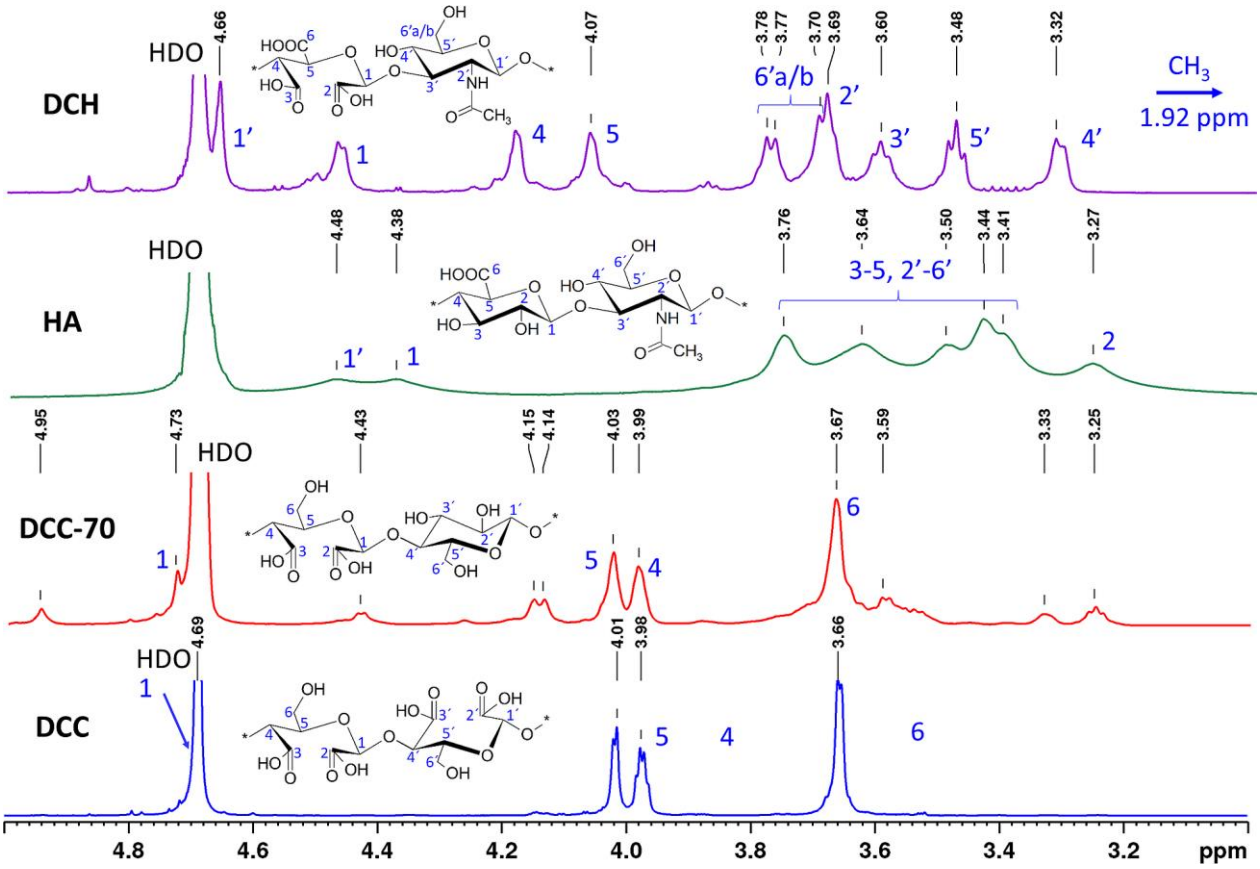

Figure 3 ^{1}H NMR spectra with the signal assignment (D_2O, 25 °C) and structural formulas of DCC, DCC-70, source sodium hyaluronate (HA), and DCH.

The molecular weight distribution of the prepared dicarboxypolysaccharides is summarized in Table 1. Note the similarity between number-average molecular weight (M_n), weight-average molecular weight (M_w), and *PDI* of DCC and DCH. The impact of the molecular weight on the characteristics of AuNPs prepared by these DCPs thus should be minimal - any observed differences must be attributed to their structural differences.

Table 1 Molecular weight analysis of the prepared DCPs, M_w is weight-average molecular weight, M_n is number-average molecular weight, *PDI* is polydispersity index and *DP* is the degree of polymerization.

	Molecular weight after DCP preparation				Molecular weight after blank AuNPs synthesis			
#	M_w (kDa)	M_n (kDa)	*PDI* (-)	*DP* (-)	M_w (kDa)	M_n (kDa)	*PDI* (-)	*DP* (-)
DCC	62.1	31.7	1.9	263	15.0	8.3	1.8	64
DCH	58.5	27.6	2.1	118	15.3	8.0	2.5	31
DCC-70	2620/73.3	1688/40.4	1.5/1.8	12254/343	1260/22.8	755/13.0	1.7/1.7	5893/107

The DCC-70 has, in comparison with other DCPs, molecular weight distribution with distinctly bimodal character (two well-separated signals were observed during GPC analysis and were analyzed separately, resulting in two values of each molecular momentum in Table 1). This is most likely a result of (i) the

presence of amorphous phase and crystalline domains in the source cellulose, which are oxidized at different rates [35] and/or (ii) recombination of freed macromolecular chains *via* the formation of intermolecular hemiacetals from partially oxidized units resulting in a significant increase in molecular weight compared to the source material. The latter seems more likely, as M_w of source cellulose was only 72 kDa, and the presence of a significant amount of intermolecular hemiacetals in DAC solutions was recently proven by NMR analysis [28].

Said molecular weight duality can be avoided by the introduction of the solubilization step after the primary oxidation [36] or by the use of the sulfonation-induced chain scission method, which predominantly targets larger molecules [29]. We have, however, opted not to perform such operations, as heterogeneous structure and high polydispersity are typical issues encountered in polysaccharides. DCC-70 thus provides an interesting opportunity to study the impact of these factors on the characteristics of AuNPs and compare them with better-defined material (DCC).

The GPC was also used to investigate the molecular weight distribution of the individual DCPs after the "blank" AuNPs synthesis, *i.e.* the synthesis in which AuNPs precursor $HAuCl_4 \cdot 3H_2O$ was substituted by the equivalent molar amount of HCl to achieve the same pH. We have resorted to this method to avoid potentially damaging GPC instrumentation by AuNPs, while still being able to study the faith of DCPs under conditions similar to those of a real synthesis. It is not surprising to see a steep decrease in all molecular momentums after the several hours of heating during blank AuNPs synthesis; the M_w of DCPs decreased roughly 4-times in the case of DCC, DCH, and the low-molecular-weight fraction of DCC-70 and about 2-times in the case a high-molecular-weight fraction of DCC-70.

3.2 Mechanism of gold salt reduction

Following the determination of the structure and properties of oxidized polysaccharides, the actual mechanism of AuNP synthesis using DCPs needs to be addressed. The classic mechanism of gold salt reduction by polysaccharides relies on the equilibrium between the hemiacetal and aldehyde group at the reducing end of the polysaccharide. When the gold salt is reduced, the aldehyde is oxidized to the carboxyl group and aldonic acid is formed. However, this reaction mechanism is not directly applicable for the DCPs, in which all available –CHO groups, including the one at the reducing end, are oxidized. The DCPs thus should be – at least in theory – non-reducing polysaccharides. Yet, this is not the case. The proposed mechanism of AuNPs reduction is shown in Scheme 1 on the example of cellulose/DCC. In essence, while the AGUs of cellulose connected by two β-(1→4) glycosidic linkages are selectively oxidized by a single molecule of $NaIO_4$ to 2,3-dialdehydes, the reducing-end group is initially oxidized to 1,3-dialdehyde [37]. During this process, C2 carbon of the end-group is eliminated as formic acid and 2 molecules of $NaIO_4$ are consumed. Then, the over-oxidation of reducing-end groups takes place [38]. The formate (C1) of the reducing-end group is eliminated as the second molecule of HCOOH. This frees the –OH group at C5 for further oxidation, leading to C5-C6 bond breaking, the release of formaldehyde (former C6), and the oxidation of –OH group at C5 to aldehyde [38]. The resulting malondialdehyde derivative is oxidized by $NaClO_2$ to the 2-hydroxymalonic (tartronic) acid. Only when tartronate attached at the reducing end of DCP is hydrolyzed, the new reducing end is formed.

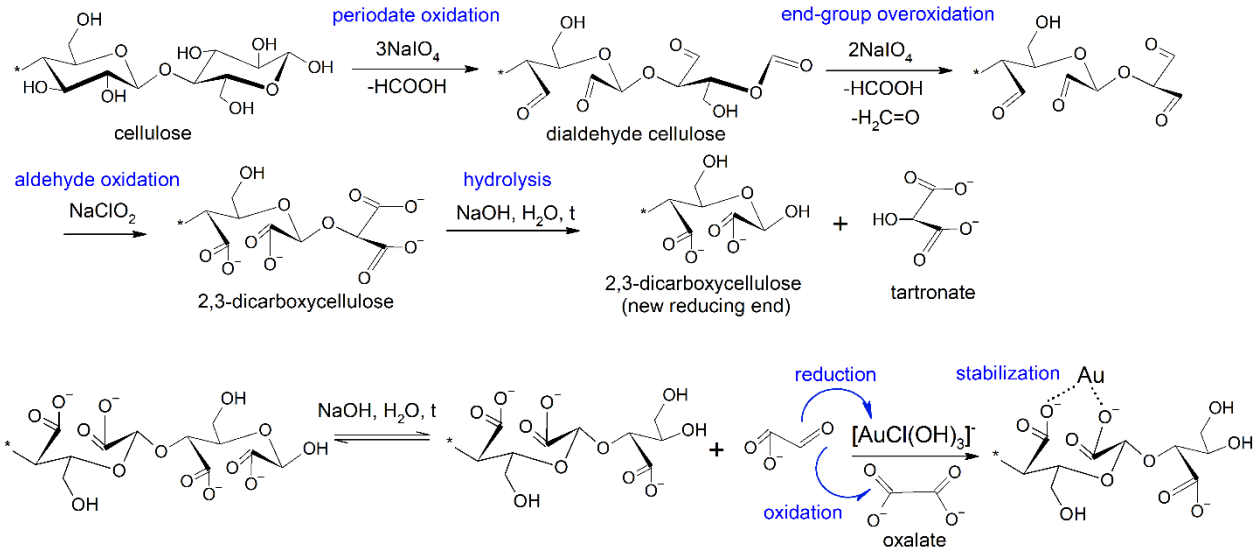

Scheme 1 Overall reaction scheme of DCC oxidation and Au salt reduction mechanism.

To prove the presence of tartronate in the reaction mixture and to support the proposed mechanism, the blank reaction, in which the $HAuCl_4 \cdot 3H_2O$ was replaced by HCl to conserve acidity, was performed. The unpurified reaction product was then lyophilized and redissolved in D_2O. ^1H NMR spectra (Figure S4) revealed besides partial hydrolysis of DCC also a very narrow signal at 5.01 ppm, which was assigned to tartronic acid based on the NMR spectra database [39]. Hence, new reducing-ends of DCC are generated in the solution by i) the hydrolysis of tartronate and ii) partial hydrolysis (chain scission) of DCC under the employed reaction conditions. After this "activation by hydrolysis" step, the DCC is capable of gold salt reduction following the modified classic polysaccharide reduction scheme. The main difference is that the absence of the bond between C2 and C3 prevents the formation of gluconic acid after the hydrolysis of the hemiacetal bond between C1 and C5. Instead, a small-molecular aldehyde is released. This molecule reduces the Au^{III} to Au^0 and is oxidized to the oxalate. Reduced gold atoms then start to form clusters, which are stabilized by functional groups of the polysaccharide chain and eventually grow into AuNPs. Unfortunately, we were unable to unequivocally prove also the presence of oxalate, as numerous other COOH signals are present in DCPs, thus masking its presence in NMR, IR, and Raman spectra. Nevertheless, the described reduction mechanism involving small-molecular aldehyde is a logical consequence of changes in the polysaccharide structure (disruption of C2-C3 bond). Note, however, that the "activation by hydrolysis" mechanism involving small molecule aldehydes applies only for oxidized units. In DCH, for example, the generated reducing-ends can be formed either by oxidized glucuronic acid or N-acetyl-D-glucosamine. While the mechanism involving small-molecule aldehyde must be expected for oxidized glucuronic acid units lacking C2-C3 bond, the (untouched) N-acetyl-D-glucosamine reducing-ends can reduce Au^{III} complexes *via* the classic reduction mechanism.

3.3 Synthesis of AuNPs by different DCPs and screening study

Because DCPs are, to the best of our knowledge, used as substrates for the preparation of AuNPs for the first time, screening of reaction conditions was performed. Summary of all obtained results can be found in SI (see Tables S1–S4 and Figures S5–S10), here we provide only an overview of major trends and

dependences. The AuNPs prepared using DCC, DCC-70, and DCH are referred to as AuDCC, AuDCC-70, and AuDCH, respectively.

Initially, the dependence of AuNPs characteristics on the duration of the synthesis was investigated (A-Series). Samples were collected each hour over five hours and analyzed. The typical red color of formed AuNPs appeared already after one hour of a reaction involving DCC and DCC-70, respectively. Contrary, only a slight tint of red-purple color became visible no sooner than after 3 h of synthesis using DCH, although a weak LSPR absorbance was observable in UV-Vis spectra already after 1 h of the synthesis (Figure S5). The wavelength of LSPR maxima of all three samples, which generally correlates with the size of AuNPs (higher wavelength = larger size), gradually decreased with the increasing duration of the synthesis. For example, the wavelength of LSPR absorbance of AuDCC-70 particles after 1 h was 540 nm but converged to 524 nm after 3 h. A similar pattern was observed for AuDCC samples (from 529 nm to 523 nm) as well as for AuDCH samples (weak absorption at 564 nm after 1 h, 537 nm after 5 h). The *ζ*-potential values of all prepared colloids measured immediately after the synthesis also showed significant differences between individual polysaccharides. While the *ζ*-potential of AuNPs prepared by DCC derivatives was fluctuating around -57.9±3.9 mV for AuDCC-70 and -66.0±1.8 mV for AuDCC, the *ζ*-potential of AuDCH changed significantly during synthesis from -87.0±4.4 mV after 1 h to -62.0±2.5 mV after 5 h (Table S2). Based on obtained data, the duration of synthesis was in the following experiments set to 3 h for DCC and DCC-70 and 5 h for DCH.

Obtained results also indicate significant differences between reduction capability and stabilizing potential of DCH compared to the DCC derivatives. It is a well-known fact that the slower reduction of Au^{III}, *i.e.* the slower the nanoparticle seed formation rate, the larger the nanoparticles became [40]. Similarly, the stronger is the stabilization potential of the polysaccharide, *i.e.* the number of functional groups in its structure capable to stabilize forming gold clusters and nanoparticles, the smaller the AuNPs will be [41]. The slower reduction observed for DCH was initially considered as a result of the slower hydrolysis of DCH chains in the reaction mixture and thus the slower generation of reducing ends. This was, however, ruled out by GPC analysis, as molecular weight moments of DCC and DCH samples were essentially the same before and after the blank synthesis, implying roughly the same number of reducing-ends forming in both polysaccharides. The most likely explanation is thus based on different compositions of reducing ends between DCC and DCH discussed in the previous section. While all reducing ends of (fully oxidized) DCC are composed of oxidized units, half of DCH reducing ends will be, statistically speaking, formed by N-acetyl-D-glucosamine ring, which needs to be opened before reduction can begin. The N-acetyl-D-glucosamine ring opening and the related hemiacetal/aldehyde equilibrium is thus likely a rate-determining step slowing the reduction of Au^{III} in comparison to DCC, in which the reactive aldehyde is bound to the chain only by a single, easily cleavable, hemiacetal bond.

To address the second major aspect influencing the AuNPs growth, the colloidal stability of AuNPs, the amount of stabilizing group in individual polysaccharide derivatives as well as their stabilizing potential has to be taken into consideration. Fully oxidized cellulose (DCC) possesses two –COOH groups per monosaccharide unit but only a single –OH group. DCC-70 contains only 70 % of –COOH groups found in DCC (1.4 –COOH group per unit on average) but has a higher amount of –OH groups (1.6 –OH group per unit on average). Because N-acetyl-D-glucosamine units remain intact during the oxidation, each

disaccharide basic structural unit of DCH contains three –COOH groups, two –OH groups, and one N-acetyl group. The overall density of –COOH groups per monosaccharide unit in the DCH is thus somewhat higher than in DCC-70 (1.5 –COOH group per monosaccharide unit on average). Although the combined amount of other functional groups (2× –OH, 1× N-acetyl group) of DCH unit is slightly lower, the N-acetyl group contains both –NH and –C=O moieties capable of stabilizing gold clusters. According to the literature, the energy of interaction between single $–COO^-$ group and gold clusters/atom(s) is ~40 kcal/mol [42], while the –OH….Au interaction is usually around 10–12 kcal/mol [30]. Recently experimentally proven hydrogen bonds between Au and H-N group had energy slightly higher than the –OH….Au interaction, about 13 kcal/mol [43], while similar interactions involving N-acetyl groups have an energy of about 18 kcal/mol [30]. The theoretical interaction energy of the oxidized DCC unit and the gold surface is thus over 90 kcal/mol (2× $–COO^-$, 1× –OH), nearly five times higher than that of non-oxidized glucose, which can be up to 20 kcal/mol in bidentate coordination [30]. Such stabilization potential is, besides adjustable composition, one of the greatest advantages of DCPs compared to unmodified polysaccharides. Hence, the theoretical stabilization potential thus decreases from DCC, over DCH to DCC-70, which corresponds to the general trend in the stability of corresponding AuNPs, expressed in terms of *ζ*-potentials.

Next, the dependence of AuNPs properties on weight concentration of given DCPs (0.2–1.2 wt%) was investigated, see B-series results in Figure S6 and Table S3. Similar patterns were observed for LSPR absorbance wavelength and *ζ*-potential values for all DCPs up to 0.8 wt% concentration. In essence, the low weight concentrations of DCP (typically 0.2 wt%) lead to the formation of AuNPs exhibiting higher LSPR maxima wavelengths and *ζ*-potential values, both of which decreased upon increasing the concentration of DCP up to 0.8 wt%. Further increase of weight concentration of DCC-70 and DCH led to the loss of LSPR absorbance value, the shift of absorbance maxima towards higher wavelengths, and related discoloration of the samples, see Figure S7. In the end, concentrations of polysaccharides for the last series were set to 0.6 wt%.

The dependence of AuNPs properties on the molar concentration of NaOH (0–10 mmol/L) was investigated in the C-series of samples (Figure S8 and Table S4). Note that the molar concentrations of NaOH are used instead of the pH values, which significantly drift after the addition of NaOH due to hydrolysis of $AuCl_4^-$. According to the literature [44], the $AuCl_4^-$ in solution undergoes both acidic and alkali hydrolysis, during which are Cl ligands replaced by H_2O or OH^- ligands, respectively, as described by Equation 1:

$$AuCl_4^- + x(OH)^- + yH_2O \rightleftharpoons [AuCl_{4-x-y}(OH)_x(H_2O)_y]^{y-1} + (x+y)Cl^- \qquad (x,y= 0\text{-}4)$$

The composition of the resulting complex with the general formula $[AuCl_{4-x-y}(OH)_x(H_2O)_y]^{y-1}$ depends on the reaction conditions, in particular on the temperature and the concentration of OH^- ions in the solution. Because the reaction time of the chloride substitution by OH^- at 95 °C is only 30 s [40], we have to assume that majority of $AuCl_4^-$ is hydrolyzed after 3–5 h at 95 °C. Regarding actual composition gold precursor complex at different pH, Wang *et* al. reported the major presence of $[AuCl_3(OH)]^-$ at pH 3, but the dominance of $[AuCl(OH)_3]^-$ at pH 6 [45]. While both $[AuCl_3(OH)]^-$ and $[AuCl(OH)_3]^-$ hydrolyze in (mildly) acidic solutions to neutral aqua complexes $[AuCl_3(H_2O)]$, $[AuCl(OH)_2(H_2O)]$ or $[Au(OH)_3(H_2O)]$, the further increase in pH leads to the formation of a rather stable $[Au(OH)_4]^-$ complex and suppression of neutral complexes formation due to high concentration of OH^- in the solution [44]. The different composition of the gold precursor is then the most likely cause of C-series results. Although AuNPs can be prepared

without NaOH (pH 3–4, dominance of $[AuCl_3(OH)]^-$ complex) results are not optimal as prepared AuNPs generally exhibit low LSPR intensity indicating poor yield, lower *ζ*-potential (-40 to -50 mV) but the higher wavelength of LSPR maxima. The best results (high LSPR absorbance value, the lowest wavelength of LSPR maxima, best yield, and increase of *ζ*-potential up to -80 mV) were obtained when NaOH concentration was set to 5 mmol/L (initial pH of the reaction between 5.5–6.0, presence of aqua complexes). Note that this concentration of NaOH was coincidentally selected already at the beginning of the study. Further increase of NaOH concentration (pH ~9, dominance of $[Au(OH)_4]^-$) led to a decrease of LSPR absorption band intensity and discoloration of AuDCC and AuDCH samples, see Figures S8 and S9. Observed maximal efficacy of AuNPs formation at slightly acidic conditions can be explained by the reduced electrostatic barrier between neutral gold aqua-complexes and negatively charged DCPs when compared to similarly negatively charged gold hydroxo complexes. The reduced electrostatic repulsion increases the availability of gold salts in the vicinity of DCP chains, which likely enhances the reduction rate. The neutral gold complexes may even bind to $–COO^-$ groups of DCPs similarly to analogical platinum(II) compounds [24,31]. Hence, we postulate that the presence of neutral complexes is of key importance for gold salt reduction by DCPs, although further analysis is required to confirm this assumption.

3.4 Properties of selected AuNPs samples prepared by different DCPs

Three types of AuNPs (one for each polysaccharide) were prepared using conditions selected in the previous section, purified, and characterized by DLS, UV-Vis, XRF, TEM (Figure 4 and S11), XRD (Figure S2), and TGA (Figure S12). All XRD diffractograms with marked Miller indices showed distinct sharp cubic gold diffraction patterns visible at 2θ around 44, 52, and 76° and broad diffraction pattern at 2θ around 17° corresponding to DCPs present on the surface of AuNPs. Besides, the LSPR, *ζ* potential, and size of newly prepared AuNPs correspond to respective samples from the screening study, which indicate good reproducibility of the synthesis.

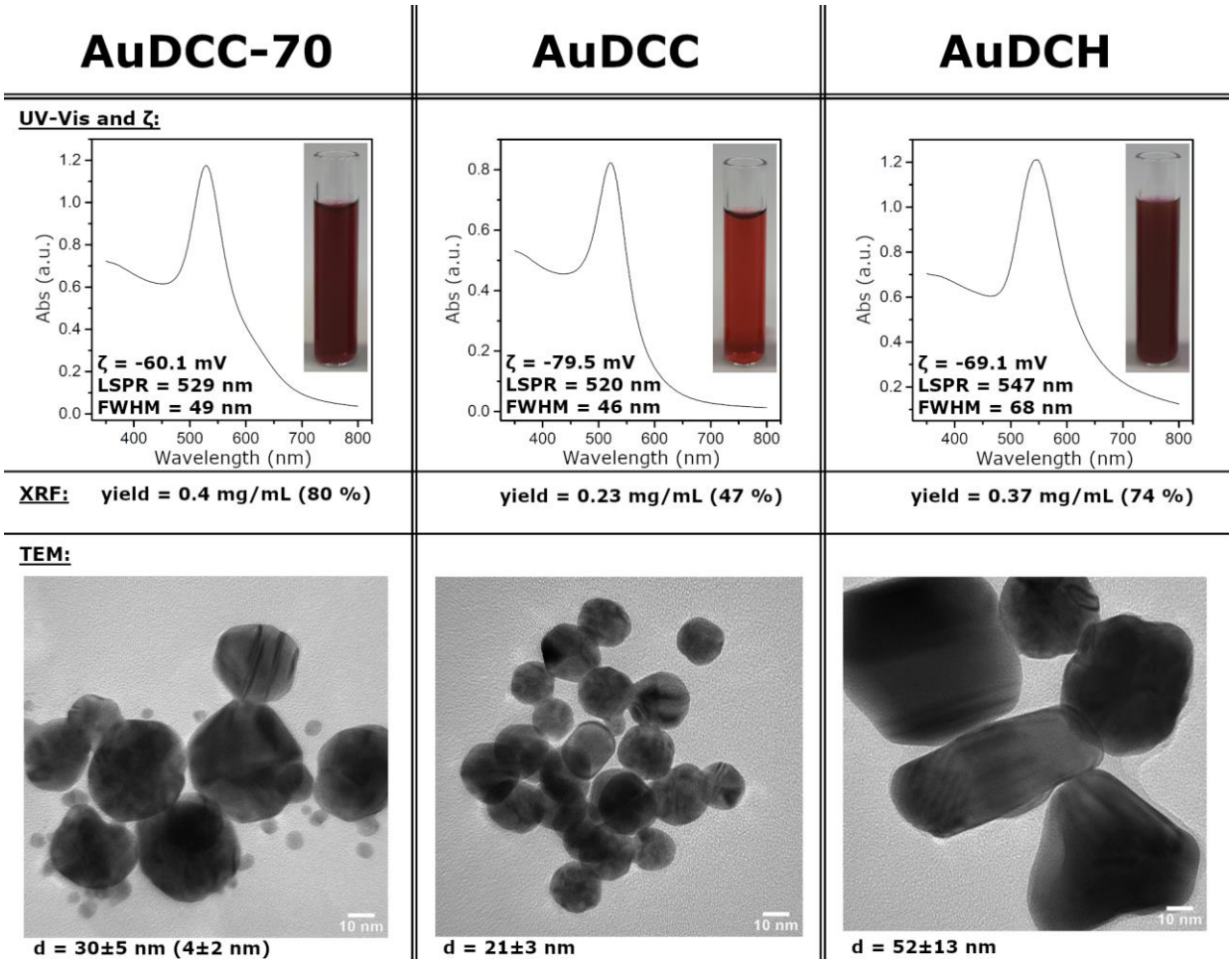

Figure 4 Properties of selected AuNPs prepared using different polysaccharide derivatives and screened parameters.

The AuDCC sample prepared using a 0.6 wt% concentration of DCC, duration of synthesis 3 h, and concentration of NaOH 5 mmol/L, featured AuNPs with rather uniform (roughly spherical) shapes and narrow size distribution of 21±3 nm (20.4 nm crystallite sizes according to XRD), the lowest observed LSPR wavelength of 520 nm, the lowest FWMH of 46 nm, the highest *ζ*-potential of -79.5±3.5 mV, and also featured the highest shell : core ratio among all samples, containing only 19 % of the gold core and 81 % DCC. On the other hand, the yield of AuDCC nanoparticles after purification was below 50 % (based on XRF), which is the lowest of all samples. The smallest sizes and highest stability of AuDCC are a result of the high reduction efficacy of DCC combined with the highest density of –COOH groups. Its high stabilization potential is likely reflected also in the largest DCP shell : Au core ratio – the higher the stabilization potential, the more of the polysaccharide remains bound to the surface and the higher is the relative thickness of the shell.

The AuDCC-70 sample was prepared using analogical conditions as AuDCC, although the weight concentration of DCC-70 was set to 0.4 wt% to maximize the LSPR absorbance value. Both LSPR wavelength (529 nm) and FWMH of 46 nm are higher than in the case of fully-oxidized DCC. The yield of AuDCC-70 nanoparticles was also higher, about 80 %. The *ζ*-potential (-60 mV) and the shell : core ratio (42 % of the

gold core and 58 % of DCC-70) of AuDCC-70 nanoparticles are lowest from all three samples, which is a direct result of the lowest amount of stabilizing groups in the DCC-70. Contrary to the uniform size distribution of AuDCC nanoparticles, AuDCC-70 colloids contain particles of two distinctly different sizes; larger ones having about 30 nm in size while smaller ones being about 4 nm large, see Figure 4. The average crystallite size was 25.5 nm. Some AuDCC-70 nanoparticles also form more irregular polyhedrons than AuDCC. Such anisotropic growth is most likely linked to the more heterogeneous composition of DCC-70 chains, where flexible and highly charged sections formed of oxidized units are interposed by stiffer and less polar non-oxidized parts. Because the presence of sub-10 nm particles is potentially interesting for catalysis, TEM analysis was also extended to other samples, see Figure S10. The number of sub-10 nm nanoparticles was found to be highest for AuDCC-70 prepared using 0.4 wt% of DCC-70 and is decreasing with an increase of DCC-70 weight concentration. Besides DCC-70 samples, only minimal amounts of small nanoparticles are observable in the AuDCC sample prepared using 0.4 wt% of DCC. There is no evidence of sub-10 nm particles in samples prepared using higher concentrations of DCC or in any AuDCH sample.

AuDCH nanoparticles (w_{DCH} = 0.4 wt%, t = 5 h, c_{NaOH} = 5 mmol/L) have the highest observed LSPR wavelength of 548 nm, FMWH of 67.5 nm, significantly larger dimensions and broader size distribution of 52±13 nm (crystallite size 33.8 nm), distinctly polyhedral shapes (hexagonal, rectangular, triangular *etc.*), while their yield (~75 %), ζ-potential of ~-70 mV and 31 % gold core and 69 % of DCH shell ratio places it between that of AuDCC and AuDCC-70 samples. All of these findings are in agreement with weaker reduction potential and medium stabilizing effect of DCH, possibly complemented by heterogeneous composition formed by oxidized (charged) glucuronic units and non-oxidized N-acetyl-D-glucosamine units resulting in the most anisotropic AuNPs growth.

3.5 Stability of AuNPs at different pH

Next, the dependence of AuNPs hydrodynamic radii and ζ-potentials on pH was investigated (Figure 5). As carboxylic groups became protonated in highly acidic conditions, the ζ-potentials of AuNPs are expectantly converging towards zero. The AuDCC colloid was the most stable, showing only a slight increase in hydrodynamic radius even at pH 2.5 and residual ζ-potential of about -20 mV. A similar result was found for AuDCH, although signs of starting particle aggregation (an increase of hydrodynamic radius) start to appear below pH 2.5. AuDCC-70 shows the lowest stability under acidic conditions; its ζ-potential approaches 0 mV and strong aggregation occur below pH 3 due to the lowest amount of $–COO^-$ groups available and thinnest shell. In contrast to the acidic environment, all prepared AuNPs remain stable even at pH 12 even though polysaccharides are known to degrade due to β-elimination processes in highly alkaline conditions [28,46]. Regarding the temporal stability, hydrodynamic radii and ζ-potentials of samples stored in the refrigerator for six months were the same (within experimental error) as those measured for freshly prepared solutions. All three samples were thus deemed to be sufficiently stable for further investigations.

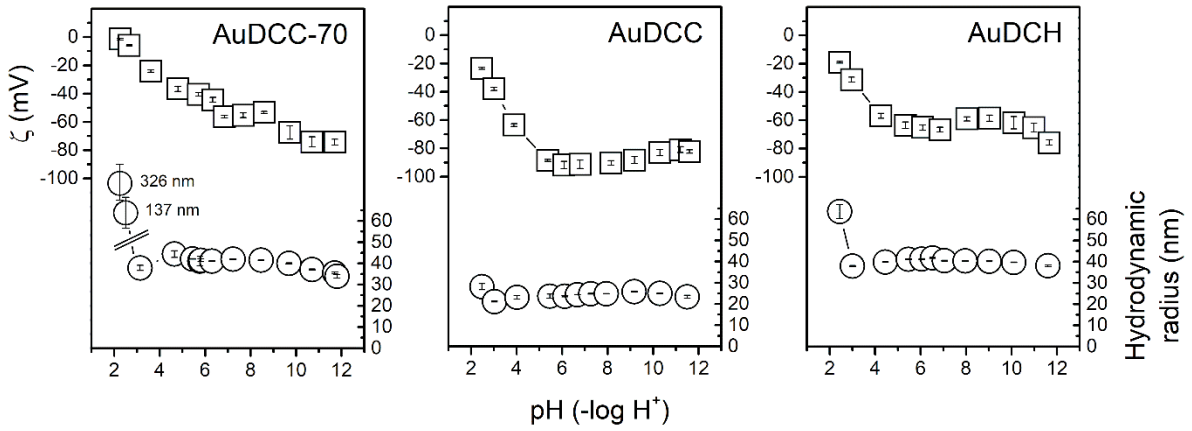

Figure 5 The ζ-potentials and hydrodynamic radii of AuNPs samples in the range of pH from 2 to 12.

3.6 Catalytic efficacy

The catalytic efficacy of prepared AuNPs was studied using the reduction of 4-nitrophenol (4-NP) to 4-aminophenol (4-AP) in the presence of sodium borohydride at ambient temperature as a model reaction, see Figure 6 [47]. Reaction progress has been observed by evaluation of decrease of 4-NP absorption intensity at 400 nm, which corresponds to decrease of its concentration with time, Figure 6A. The reduction does not occur in the absence of a gold catalyst, even when replaced by the same amount of respective DCP, see Figure 6B (blank; black line). The addition of 20 µg of AuNPs immediately initiates the reduction reaction, which follows the pseudo-first-order kinetics, as can be seen from the linear dependence of $ln(c_t/c_0)$ on reaction time, Figure 6C. The slope of the $ln(c_t/c_0)$ plotted vs. time was used to calculate the reaction rate constants (k). The turnover frequency (TOF), which corresponds to moles of reactant converted by the molar amount of catalyst per minute, was calculated concerning the initial concentration of 4-NP as recommended in the literature [34]. Obtained results are also compared with other reported AuNPs systems involving polysaccharides (Table 2).

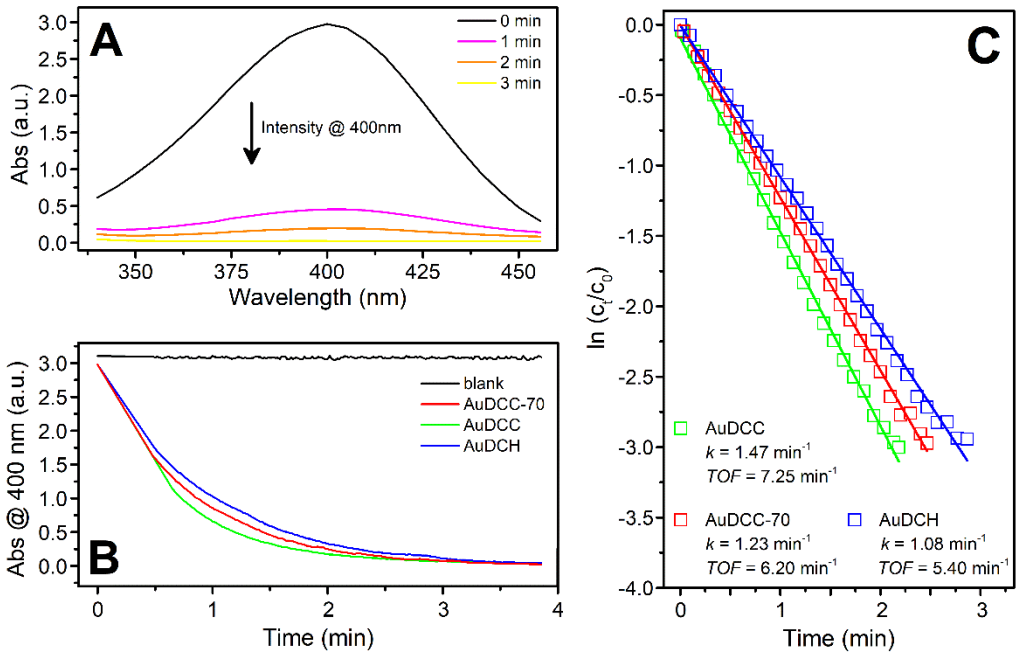

Figure 6 Catalytic efficacy of prepared AuNPs. Part A shows the decrease of intensity of 4-NP absorption upon its AuNPs-catalyzed reduction by $NaBH_4$. Part B shows the progress of reduction catalyzed by different AuNPs in terms of decreasing intensity of 4-NP absorption band at 400 nm over the course of 4 min (blank sample contains 4-NP and $NaBH_4$ without AuNPs). Part C shows the dependence of $ln(c_t/c_0)$ on reaction time as well as calculated rate constants (k) and turn over frequencies (TOF); c_0 is the initial concentration of 4-NP, c_t is the concentration of 4-NP in time t.

The reduction of 4-NP is finished within three minutes since the addition of AuNPs in all cases. The full conversion was determined based on the constant absorbance readings at 400 nm. The highest reaction rate constant from tested materials is 1.47 min^{-1} for AuDCC, followed by 1.23 min^{-1} for AuDCC-70 and 1.08 min^{-1} for AuDCH. TOF values follow the same trend; they are between 7.3 min^{-1} (AuDCC) and 5.4 min^{-1} (AuDCH). The k and TOF values of the AuDCC sample are about one-third higher than those of AuDCH. This is not surprising as large and irregularly shaped AuDCH nanoparticles are the least suited for catalysis. Interestingly, the presence of sub-10 nm particles in the AuDCC-70 sample does not improve its catalytic activity over that of AuDCC, which is probably being balanced by the reduced performance of larger nanoparticles.

Table 2 Comparison of conditions of 4-NP reduction by different systems. *TW* stands for this work.

Catalyst	n_{Au} (mmol)	$n_{4\text{-}NP}$ (mmol)	$c_{4\text{-}NP}$ (mmol/L)	Conversion t (min)	TOF (min^{-1})	k (min^{-1})	Ref.
AuDCC	1.02×10^{-4}	5×10^{-4}	0.17	2.8	7.3	1.47	*TW*
AuDCC-70	1.02×10^{-4}	5×10^{-4}	0.17	2.8	6.2	1.23	*TW*
AuDCH	1.02×10^{-4}	5×10^{-4}	0.17	3.0	5.4	1.08	*TW*

cMNPs@Au20	5.03×10^{-6}	5×10^{-4}	0.16	2	49.7	1.85	[33]
Au/chitosan/Fe_3O_4	5.00×10^{-6}	1×10^{-2}	0.48	1.5	2.1	2.83	[47]
AuNPs@CSNFs	1.00×10^{-5}	1.5×10^{-3}	0.05	16	9.4	0.35	[48]
Au/CNF	4.32×10^{-4}	4×10^{-4}	0.1	5	0.33	5.43	[49]
AuNPs/AOBC	1.45×10^{-4}	1.5×10^{-2}	0.3	24	4.33	0.13	[50]

Generally, the catalytic efficacy of all three prepared AuNPs is comparable or better than those previously reported for various gold nanoparticles prepared using polysaccharides [33,47–50]. Reported reaction constants for 4-NP reduction are between 0.13 min^{-1} and 5.43 min^{-1}, which put our results in the middle of the field. On the other hand, reported TOF values, which take into consideration the amount of catalyst, are among the highest, which indicates the rather good catalytic performance of our systems. Note, however, that this may be to a certain extent caused by different experimental conditions.

3.7 The SERS efficacy

To evaluate whether prepared nanoparticles are SERS-active, 50 µL of the solutions containing the NAC, AuNPs, or both were dried on an aluminum substrate and the Raman signal was measured. Although signals of neat NAC (50 µL of 2 mg/mL solution dried on the substrate) and AuNPs themselves (50 µL of 1 mg/mL colloid dried on the substrate) were below the detection limit, characteristic bands of NAC incubated overnight with AuNPs are clearly visible in Figure 7. Compared to spectra of pure NAC powder measured under the same conditions (not shown), bands of NAC enhanced by AuNPs are generally shifted towards a higher wavenumber. For instance, the characteristic vibrational band of –SH group at 2572 cm^{-1} is shifted by 13 cm^{-1} compared to powdered NAC (2559 cm^{-1}); the band at 1734 cm^{-1} corresponding to the ν C=O stretching mode of the carboxyl groups is shifted by 19 cm^{-1} (powdered NAC 1715 cm^{-1}); intensive Raman band at 1657 cm^{-1} and its small shoulder at 1611 cm^{-1} corresponding to vibration modes of amide I of the peptide group (stretching of the C=O group) are shifted by 16 cm^{-1} (1631 cm^{-1} powdered NAC) and by 6 cm^{-1} (powdered NAC 1605 cm^{-1}), respectively. Observed wavenumber shifts are most likely caused by the formation of weak interactions between the analyte and surface of AuNPs upon the adsorption. Other bands observable in AuNPs-enhanced SERS spectra include deformation vibrations of δ-CH_2- and δ_s-CH_3 and rocking vibration of ρ-CH_3 at 1420 cm^{-1}, 1378 cm^{-1} and 1040 cm^{-1} and vibration amide III mode (broad band at 1283 cm^{-1}).

Although it is impossible to evaluate the absolute signal enhancement factor provided by AuNPs because Raman signals of neat NAC are below the detection limit, the relative signal enhancement between the samples can be evaluated by comparison of signal intensities. Recall, that the intensity of Raman signal increase provided by AuNPs depends on their size (maximum effectivity is reached for ~50 nm nanoparticles), but more importantly, on their shape (the more irregular, the better) [14]. The smallest observed enhancement was obtained for uniform and small AuDCC nanoparticles. Interestingly, AuDCC-70 nanoparticles were only marginally better than AuDCC ones despite having about 50 % larger dimensions. In contrast, the irregular shape of AuDCH in combination with their almost ideal size and, possibly, also different dielectric constant of DCH vs. DCC led to 9× stronger Raman signals on average

compared to AuDCC. AuDCH nanoparticles are thus particularly promising candidates for SERS-based sensing applications.

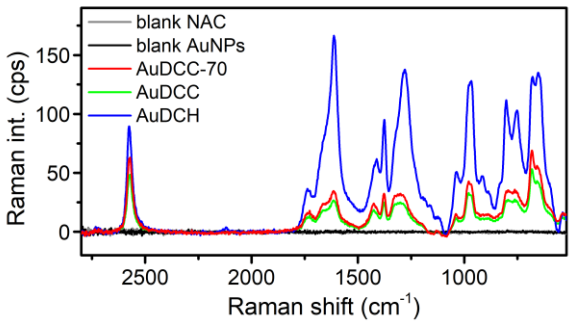

Figure 7 Comparison of SERS of NAC signal provided by AuDCC, AuDCC-70, and AuDCH on an aluminum substrate. Blank samples contained 0.1 mg/mL AuNPs and 2 mg/mL NAC.

4. Conclusion

The DCPs are capable of reduction of gold salts to gold nanoparticles due to the formation of new reducing ends at increased temperature, *i.e. via* the "activation by hydrolysis" mechanism. While the rate of the gold salt reduction is dependent on the structure of the DCP's reducing end, the colloidal stability of the AuNPs is related to the amount and type of stabilizing groups in polysaccharide structure, *i.e.* on the nature of source polysaccharide as well as on conditions of regioselective oxidation. Comparison of three different source materials revealed that: i) the well-defined and homogenous structure of fully oxidized cellulose (DCC), together with highest stabilization potential (highest density of –COOH groups) supports isotropic growth of nanoparticles resulting in the smallest AuNPs (20 nm) with a narrow size distribution, uniform and roughly spherical shape, the highest stability in a broad range of pH, and the best catalytic efficacy for the reduction of 4-NP from all three tested samples. ii) The use of partially oxidized cellulose with significant molecular weight polydispersity and lower stabilization potential compared to fully oxidized cellulose led to the preparation of the mixture of 4 nm and 30 nm large nanoparticles, which were the least stable from all samples and some of which had distinctly irregular shapes. The formation of smaller particles was likely induced by a higher molecular weight fraction of DCC-70, although the exact mechanism is unclear. iii) Slower reduction rates given by the presence of non-oxidized N-acetylglucosamine units in DCH, together with the lower stabilization potential per unit compared to DCC induce growth of larger (~50 nm) and distinctly irregular nanoparticles, which excel in increasing SERS efficacy. A rather anisotropic topology of AuDCH nanoparticles is attributed to the DCH structure composed of alternating highly charged oxidized moieties and less polar non-oxidized units bearing several different functional groups. To summarize, the controlled oxidative modification of source polysaccharides opens new possibilities for the preparation of AuNPs optimized for different applications.

Acknowledgment

This work was supported by the Ministry of Education, Youth and Sports of the Czech Republic – DKRVO (RP/CPS/2022/007) and Internal Grant Agency of TBU - IGA/CPS/2020/003 and IGA/CPS/2021/002. We

acknowledge Josef Dadok National NMR Centre of CIISB, Instruct-CZ Centre, supported by the Ministry of Education, Youth and Sports of the Czech Republic (LM2018127).

Notes

The authors declare no competing financial interest.

Associated Information

Supplementary Information is available: Contains basic qualitative analysis (FT-IR) of prepared DCPs and codification of all AuNPs samples prepared within the screening study, their spectral properties, stability, additional TEM micrographs and macroscopic pictures. TGA of production AuNPs samples and NMR of DCC after blank synthesis is also included.

***CRediT* author statement**

A. Vávrová: Investigation, Validation, Writing – Original Draft. **T. Čapková**: Investigation, Formal Analysis, Writing – Review & Editing. **I. Kuřitka**: Supervision, Funding Acquisition. **J. Vícha**: Investigation, Conceptualization, Data Curation, Writing – Original Draft, Writing – Review & Editing. **L. Münster**: Investigation, Methodology, Visualization, Writing – Original Draft, Writing – Review & Editing, Project Administration.

References:

[1] M.C. Daniel, D. Astruc, Gold Nanoparticles: Assembly, Supramolecular Chemistry, Quantum-Size-Related Properties, and Applications toward Biology, Catalysis, and Nanotechnology, Chem. Rev. 104 (2004) 293–346. https://doi.org/10.1021/cr030698+.

[2] S. Lepinay, A. Staff, A. Ianoul, J. Albert, Improved detection limits of protein optical fiber biosensors coated with gold nanoparticles, Biosens. Bioelectron. 52 (2014) 337–344. https://doi.org/10.1016/j.bios.2013.08.058.

[3] J.F. Hainfeld, D.N. Slatkin, T.M. Focella, H.M. Smilowitz, Gold nanoparticles: a new X-ray contrast agent, Br. J. Radiol. 79 (2006) 248–253. https://doi.org/10.1259/bjr/13169882.

[4] J. Comenge, C. Sotelo, F. Romero, O. Gallego, A. Barnadas, T.G.-C. Parada, F. Domínguez, V.F. Puntes, Detoxifying Antitumoral Drugs via Nanoconjugation: The Case of Gold Nanoparticles and Cisplatin, PLOS ONE. 7 (2012) e47562. https://doi.org/10.1371/journal.pone.0047562.

[5] L.M. Kustov, Catalytic properties of supported gold nanoparticles in organic syntheses, Russ. Chem. Bull. 62 (2013) 869–877. https://doi.org/10.1007/s11172-013-0119-9.

[6] C. Louis, O. Pluchery, Gold Nanoparticles for Physics, Chemistry and Biology, Imperial College Press, 2012. https://doi.org/10.1142/p815.

[7] I.Ch. Oladipo, A. Lateef, J.A. Elegbede, M.A. Azeez, T.B. Asafa, T.A. Yekeen, A. Akinboro, E.B. Gueguim-Kana, L.S. Beukes, T.O. Oluyide, O.R. Atanda, Enterococcus species for the one-pot biofabrication of gold nanoparticles: Characterization and nanobiotechnological applications, J. Photochem. Photobiol. B. 173 (2017) 250–257. https://doi.org/10.1016/j.jphotobiol.2017.06.003.

[8] J.A. Elegbede, A. Lateef, Green Synthesis of Silver (Ag), Gold (Au), and Silver–Gold (Ag–Au) Alloy Nanoparticles: A Review on Recent Advances, Trends, and Biomedical Applications, in: D.K. Verma, M.R. Goyal, H.A.R. Suleria (Eds.), Nanotechnol. Nanomater. Appl. Food Health Biomed. Sci., 1st ed., Apple Academic Press, Series statement: Innovations in agricultural and biological engineering, 2019: pp. 3–89. https://doi.org/10.1201/9780429425660-1.

[9] I.C. Oladipo, A. Lateef, M.A. Azeez, T.B. Asafa, T.A. Yekeen, S.B. Ogunsona, H.M. Irshad, S.H. Abbas, Antidiabetic properties of phytosynthesized gold nanoparticles (AuNPs) from *Datura stramonium* seed, IOP Conf. Ser. Mater. Sci. Eng. 805 (2020) 012035. https://doi.org/10.1088/1757-899X/805/1/012035.

[10] R.A. Sperling, P. Rivera Gil, F. Zhang, M. Zanella, W.J. Parak, Biological applications of gold nanoparticles, Chem. Soc. Rev. 37 (2008) 1896. https://doi.org/10.1039/b712170a.

[11] F. Tian, F. Bonnier, A. Casey, A.E. Shanahan, H.J. Byrne, Surface enhanced Raman scattering with gold nanoparticles: effect of particle shape, Anal Methods. 6 (2014) 9116–9123. https://doi.org/10.1039/C4AY02112F.

[12] R.E. Darienzo, O. Chen, M. Sullivan, T. Mironava, R. Tannenbaum, Au nanoparticles for SERS: Temperature-controlled nanoparticle morphologies and their Raman enhancing properties, Mater. Chem. Phys. 240 (2020) 122143. https://doi.org/10.1016/j.matchemphys.2019.122143.

[13] S. Hong, X. Li, Optimal Size of Gold Nanoparticles for Surface-Enhanced Raman Spectroscopy under Different Conditions, J. Nanomater. 2013 (2013) 1–9. https://doi.org/10.1155/2013/790323.

[14] F. Hao, C.L. Nehl, J.H. Hafner, P. Nordlander, Plasmon Resonances of a Gold Nanostar, Nano Lett. 7 (2007) 729–732. https://doi.org/10.1021/nl062969c.

[15] A. Corma, H. Garcia, Supported gold nanoparticles as catalysts for organic reactions, Chem. Soc. Rev. 37 (2008) 2096. https://doi.org/10.1039/b707314n.

[16] A.S.K. Hashmi, Gold-Catalyzed Organic Reactions, Chem. Rev. 107 (2007) 3180–3211. https://doi.org/10.1021/cr000436x.

[17] A. Alshammari, V.N. Kalevaru, Supported Gold Nanoparticles as Promising Catalysts, in: N.K. Mishra (Ed.), Catal. Appl. Nano-Gold Catal., InTech, 2016. https://doi.org/10.5772/64394.

[18] P. Senthil Kumar, I. Pastoriza-Santos, B. Rodríguez-González, F. Javier García de Abajo, L.M. Liz-Marzán, High-yield synthesis and optical response of gold nanostars, Nanotechnology. 19 (2008) 015606. https://doi.org/10.1088/0957-4484/19/01/015606.
[19] J. Xie, Q. Zhang, J.Y. Lee, D.I.C. Wang, The Synthesis of SERS-Active Gold Nanoflower Tags for *In Vivo* Applications, ACS Nano. 2 (2008) 2473–2480. https://doi.org/10.1021/nn800442q.
[20] J. Li, J. Wu, X. Zhang, Y. Liu, D. Zhou, H. Sun, H. Zhang, B. Yang, Controllable Synthesis of Stable Urchin-like Gold Nanoparticles Using Hydroquinone to Tune the Reactivity of Gold Chloride, J. Phys. Chem. C. 115 (2011) 3630–3637. https://doi.org/10.1021/jp1119074.
[21] A. Corma, P. Concepcion, I. Dominguez, V. Forne, M. Sabater, Gold supported on a biopolymer (chitosan) catalyzes the regioselective hydroamination of alkynes, J. Catal. 251 (2007) 39–47. https://doi.org/10.1016/j.jcat.2007.07.021.
[22] R.A. Sperling, W.J. Parak, Surface modification, functionalization and bioconjugation of colloidal inorganic nanoparticles, Philos. Trans. R. Soc. Math. Phys. Eng. Sci. 368 (2010) 1333–1383. https://doi.org/10.1098/rsta.2009.0273.
[23] E. Maekawa, T. Koshijima, Properties of 2,3-dicarboxy cellulose combined with various metallic ions, J. Appl. Polym. Sci. 29 (1984) 2289–2297. https://doi.org/10.1002/app.1984.070290705.
[24] L. Münster, M. Fojtů, Z. Capáková, M. Muchová, L. Musilová, T. Vaculovič, J. Balvan, I. Kuřitka, M. Masařík, J. Vícha, Oxidized polysaccharides for anticancer-drug delivery: What is the role of structure?, Carbohydr. Polym. 257 (2021) 117562. https://doi.org/10.1016/j.carbpol.2020.117562.
[25] H. He, R. Chen, L. Zhang, W. Shen, Growth of gold nanoparticles on cellulose nanofibers, Cellulose. 27 (2020) 5041–5053. https://doi.org/10.1007/s10570-020-03142-5.
[26] G. Xiao, Y. Wang, H. Zhang, Z. Zhu, S. Fu, Dialdehyde cellulose nanocrystals act as multi-role for the formation of ultra-fine gold nanoparticles with high efficiency, Int. J. Biol. Macromol. 163 (2020) 788–800. https://doi.org/10.1016/j.ijbiomac.2020.07.057.
[27] K. Zhang, M. Shen, H. Liu, S. Shang, D. Wang, H. Liimatainen, Facile synthesis of palladium and gold nanoparticles by using dialdehyde nanocellulose as template and reducing agent, Carbohydr. Polym. 186 (2018) 132–139. https://doi.org/10.1016/j.carbpol.2018.01.048.
[28] L. Münster, J. Vícha, J. Klofáč, M. Masař, P. Kucharczyk, I. Kuřitka, Stability and aging of solubilized dialdehyde cellulose, Cellulose. 24 (2017) 2753–2766. https://doi.org/10.1007/s10570-017-1314-x.
[29] L. Münster, B. Hanulíková, M. Machovský, F. Latečka, I. Kuřitka, J. Vícha, Mechanism of sulfonation-induced chain scission of selectively oxidized polysaccharides, Carbohydr. Polym. 229 (2020) 115503. https://doi.org/10.1016/j.carbpol.2019.115503.
[30] H. Schmidbaur, H.G. Raubenheimer, L. Dobrzańska, The gold–hydrogen bond, Au–H, and the hydrogen bond to gold, Au···H–X, Chem. Soc. Rev. 43 (2013) 345–380. https://doi.org/10.1039/C3CS60251F.
[31] L. Münster, M. Fojtů, Z. Capáková, T. Vaculovič, M. Tvrdoňová, I. Kuřitka, M. Masařík, J. Vícha, Selectively oxidized cellulose with adjustable molecular weight for controlled release of platinum anticancer drugs, Biomacromolecules. 20 (2019) 1623–1634. https://doi.org/10.1021/acs.biomac.8b01807.
[32] F. Jiang, Jerry.L. Dallas, B.K. Ahn, Y.-L. Hsieh, 1D and 2D NMR of nanocellulose in aqueous colloidal suspensions, Carbohydr. Polym. 110 (2014) 360–366. https://doi.org/10.1016/j.carbpol.2014.03.043.
[33] Z. Medříková, P. Jakubec, V. Ranc, A. Bakandritsos, J. Kašlík, R. Zbořil, Carboxymethylcellulose-based magnetic Au or Ag nanosystems: Eminent candidates in catalysis, sensing applications based on SERS, and electrochemistry, Appl. Mater. Today. 14 (2019) 143–150. https://doi.org/10.1016/j.apmt.2018.12.001.
[34] S. Kozuch, J.M.L. Martin, “Turning Over” Definitions in Catalytic Cycles, ACS Catal. 2 (2012) 2787–2794. https://doi.org/10.1021/cs3005264.

[35] P. Calvini, G. Conio, E. Princi, S. Vicini, E. Pedemonte, Viscometric determination of dialdehyde content in periodate oxycellulose Part II. Topochemistry of oxidation, Cellulose. 13 (2006) 571–579. https://doi.org/10.1007/s10570-005-9035-y.
[36] U.-J. Kim, M. Wada, S. Kuga, Solubilization of dialdehyde cellulose by hot water, Carbohydr. Polym. 56 (2004) 7–10. https://doi.org/10.1016/j.carbpol.2003.10.013.
[37] K.A. Kristiansen, A. Potthast, B.E. Christensen, Periodate oxidation of polysaccharides for modification of chemical and physical properties, Carbohydr. Res. 345 (2010) 1264–1271. https://doi.org/10.1016/j.carres.2010.02.011.
[38] A.S. Perlin, Glycol-Cleavage Oxidation, in: D. Horton (Ed.), Adv. Carbohydr. Chem. Biochem., Academic Press, 2006: pp. 183–250. https://doi.org/10.1016/S0065-2318(06)60005-X.
[39] SpectraBase, SpectraBase Compound ID=3DjgOK9dbap https://spectrabase.com/compound/3DjgOK9dbap, (n.d.).
[40] M. Wuithschick, A. Birnbaum, S. Witte, M. Sztucki, U. Vainio, N. Pinna, K. Rademann, F. Emmerling, R. Kraehnert, J. Polte, Turkevich in New Robes: Key Questions Answered for the Most Common Gold Nanoparticle Synthesis, ACS Nano. 9 (2015) 7052–7071. https://doi.org/10.1021/acsnano.5b01579.
[41] L. Sun, J. Li, J. Cai, L. Zhong, G. Ren, Q. Ma, One pot synthesis of gold nanoparticles using chitosan with varying degree of deacetylation and molecular weight, Carbohydr. Polym. 178 (2017) 105–114. https://doi.org/10.1016/j.carbpol.2017.09.032.
[42] A.H. Pakiari, Z. Jamshidi, Interaction of Amino Acids with Gold and Silver Clusters, J. Phys. Chem. A. 111 (2007) 4391–4396. https://doi.org/10.1021/jp070306t.
[43] M. Straka, E. Andris, J. Vícha, A. Růžička, J. Roithová, L. Rulíšek, Spectroscopic and Computational Evidence of Intramolecular AuI···H+−N Hydrogen Bonding, Angew. Chem. 131 (2019) 2033–2038. https://doi.org/10.1002/ange.201811982.
[44] I.V. Mironov, E.V. Makotchenko, The Hydrolysis of AuCl4−and the Stability of Aquachlorohydroxocomplexes of Gold(III) in Aqueous Solution, J. Solut. Chem. 38 (2009) 725–737. https://doi.org/10.1007/s10953-009-9400-9.
[45] S. Wang, K. Qian, X. Bi, W. Huang, Influence of Speciation of Aqueous HAuCl4 on the Synthesis, Structure, and Property of Au Colloids, J. Phys. Chem. C. 113 (2009) 6505–6510. https://doi.org/10.1021/jp811296m.
[46] A. Potthast, S. Schiehser, T. Rosenau, M. Kostic, Oxidative modifications of cellulose in the periodate system – Reduction and beta-elimination reactions 2nd ICC 2007, Tokyo, Japan, October 25–29, 2007, Holzforschung. 63 (2008) 12–17. https://doi.org/10.1515/HF.2009.108.
[47] Y. Qiu, Z. Ma, P. Hu, Environmentally benign magnetic chitosan/Fe_3O_4 composites as reductant and stabilizer for anchoring Au NPs and their catalytic reduction of 4-nitrophenol, J Mater Chem A. 2 (2014) 13471–13478. https://doi.org/10.1039/C4TA02268H.
[48] H. Koga, E. Tokunaga, M. Hidaka, Y. Umemura, T. Saito, A. Isogai, T. Kitaoka, Topochemical synthesis and catalysis of metal nanoparticles exposed on crystalline cellulose nanofibers, Chem. Commun. 46 (2010) 8567–8569. https://doi.org/10.1039/C0CC02754E.
[49] M. Gopiraman, D. Deng, S. Saravanamoorthy, I.-M. Chung, I. Soo Kim, Gold, silver and nickel nanoparticle anchored cellulose nanofiber composites as highly active catalysts for the rapid and selective reduction of nitrophenols in water, RSC Adv. 8 (2018) 3014–3023. https://doi.org/10.1039/C7RA10489H.
[50] M. Chen, H. Kang, Y. Gong, J. Guo, H. Zhang, R. Liu, Bacterial Cellulose Supported Gold Nanoparticles with Excellent Catalytic Properties, ACS Appl. Mater. Interfaces. 7 (2015) 21717–21726. https://doi.org/10.1021/acsami.5b07150.